DOI: https://doi.org/10.14311/TPFM.2025.025

COMPUTATIONALLY VIABLE APPROACH TO TWIN-FLUID INTERNAL MIXING ATOMIZER MODELING

P. Novosad, M. Malý, O. Cejpek, J. Hájek, O. Hájek, J. Jedelský

Energy Institute, Faculty of Mechanical Engineering, Brno University of Technology, Technická 2896/2, 616 69 Brno, Czech Republic

Abstract

Internal mixing atomizers utilize the multiphase mixture expansion for liquid atomization not requiring fine channels prone to clogging. This study focuses on the issue of multiphase mixture formation and the effect of its character on the resulting spray formation phenomena. It employs Computational Fluid Dynamics (CFD) approaches with the implementation of Volume of Fluid (VOF) and Large Eddy Simulation (LES) methods in ANSYS FLUENT software. This publication provides a novel computational framework that reduces the computational cost while maintaining the accuracy of capturing key effects. Dividing the computational domain into separate sections for the mixing chamber and the detailed investigation of the discharge orifice. The results of this study show a strong correlation between simulation results and experimental measurements, providing insight into the internal flow mechanisms and also serving as a basis for improving the design process of these atomizers.

Keywords: Internal mixing, Atomizer, Computational Fluid Dynamics, Multiphase Flow, Volume of Fluid

1 Introduction

Internal-mixing atomizers utilize the energy of the entering gas to form a high-pressure, two-phase mixture that expands as it exits the atomizer through the discharge orifice, fragmenting into a mixture of ligaments and droplets of a wide range of sizes. Predicting the behavior of these atomizers is often difficult due to the complex interactions of the multiphase mixture flow structures in the mixing chamber.

In order to predict the performance of such atomizers, it is necessary to gather information about the behavior of the multiphase mixture inside the atomizer. In this aspect, the experimental methods face limitations. These are typical optical methods, which are used to measure the atomized spray properties and have difficulty monitoring high-speed processes with small dimensions inside the atomizer. Studies such as [1] and [2] focus mainly on determining the operating regimes of atomizers, but are unable to capture the phenomena causing these regimes, so they focus on the description based on the operating parameters of the atomizer. These are usually expressed in the form of velocities or dimensionless numbers describing the ratio of different types of energy or forces acting in a multiphase mixture. This is not a very effective approach because the atomizer behavior is strongly dependent on the exact geometry.

An alternative approach to capturing these phenomena is using computational fluid dynamics (CFD) simulations, which allow detailed investigation of internal flow and phase interactions. This method, however, presents several challenges. Primarily, there is the computational demand required to achieve an accurate representation of the multiphase mixture flow. Publications typically try to avoid this problem by isolating an individual phenomenon, which simplifies the problem significantly. [3] compares the results of CFD simulation for discharge of a singular air bubble with experimental measurement. [4] monitors the nature of the flow in the mixing chamber and discharge. However, the two-phase mixture in the atomizer is formed by initialization and not created by parameters of fluids entering the atomizer. [5] investigates an atomizer with internal mixing, and the internal flow structures are not formed as a result of initialization but only by boundary conditions. However, it is an atomizer of a specific kind with a long discharge orifice in which a liquid film forms on the walls and is torn by the viscous forces of the surrounding air core reminiscent of an air blast atomizer. This problem exploits symmetry, which can over-stabilize the flow.

Publications such as [6] and [7] have used CFD to model liquid atomization and concluded that, given sufficient grid resolution (at least 8 elements per drop diameter) and time step size, this approach follows the similar trends expressed in experimental measurements.

2 Methods

To solve the multiphase flow problem, we assume the Eulerian continuum approach. Since the individual phases interact strongly, the flow is highly turbulent, and it is necessary to capture this turbulence with high accuracy. Reynolds-averaged Navier-Stokes (RANS) turbulence formulation approach seems to over-stabilize the phase interface. Therefore, Large Eddy Simulation turbulence modeling approach is used. The fluid flow is described by a group of Navier-Stokes equations describing the laws of conservation of mass in equation 1 and momentum in equation 2.

$$\frac{\partial \rho}{\partial t} + \frac{\partial}{\partial x_i}(\rho v_i) = 0 \tag{1}$$

$$\frac{\partial v_i}{\partial t} + v_j \frac{\partial v_i}{\partial x_j} = -\frac{1}{\rho}\frac{\partial p}{\partial x_i} + \frac{\mu}{\rho}\frac{\partial^2 v_i}{\partial x_j \partial x_j} + \frac{\mu}{3\rho}\frac{\partial^2 v_i}{\partial x_i \partial x_i} + \rho g_i + a_i \tag{2}$$

Where ρ is the fluid density, t is the time, x_i and v_i are the i-th components of direction and velocity, respectively. p is the fluid static pressure, μ is the dynamic viscosity of the fluid, g_i is the i-th component of the gravitational acceleration, and a_i is the i-th component of the local volumetric acceleration acting on the fluid.

In order to describe the compressible flow, the conservation of energy equation 3, where E is the mechanical energy, must be introduced. Due to the high pressure and velocity gradients in the mixing chamber outlet, it is necessary to consider the equation in the form of a mechanical energy conservation law including the kinetic energy component to maintain accuracy.

$$\frac{\partial E}{\partial t} + v_i \frac{\partial E}{\partial x_i} + v_i \frac{\partial p}{\partial x_i} = -\frac{1}{\rho}\frac{\partial q_i}{\partial x_i} + \frac{S}{\rho} + \frac{\mu}{\rho}\frac{\partial^2 v_i}{\partial x_j \partial x_j} + \rho g_i v_i \tag{3}$$

The explicit formulation of the Volume of Fluid model is used for the description of the individual phases, which introduces a volume fraction variable α defined according to equation 4, which takes values from 0 to 1. This is used for a continuous description of the changes in the effective fluid parameters. Those are thermal conductivity k in equation 5, dynamic viscosity in 6, density in 7, and specific heat in 8. And they are considered linearly dependent on the concentration of the individual phases. With subscript l referring to liquid properties and g referring to gas properties.

$$\alpha = \frac{V_l}{V_l + V_g} \tag{4}$$

$$k = \alpha k_l + (1-\alpha) k_g \tag{5}$$

$$\mu = \alpha \mu_l + (1-\alpha) \mu_g \tag{6}$$

$$\rho = \alpha \rho_l + (1-\alpha) \rho_g \tag{7}$$

$$c_v = \frac{1}{\rho}\left(\alpha \rho_l c_{v,l} + (1-\alpha)\rho_g c_{v,g}\right) \tag{8}$$

The interface is tracked by solving the continuity equation for the volume fraction of each phase. A piecewise-linear integration scheme is used in the elements near the interface. This scheme is used to determine the fluxes on the surfaces between the elements and considers the area occupied by each phase as if the interface passed through the element in a plane, as shown in Figure 1. It represents the most accurate scheme available.

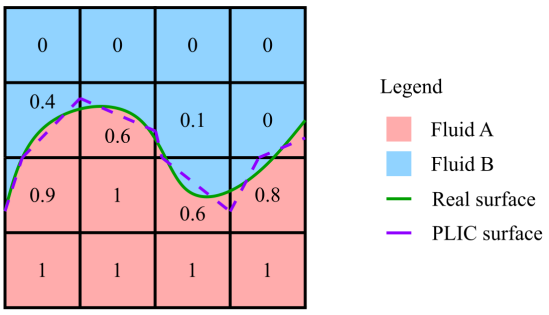

Figure 1: Piecewise-Linear Interface Construction (PLIC) Scheme approach to interface modeling

The continuum surface stress model is used to capture the effect of surface tension. It manifests itself as local volumetric acceleration in the equation 2 and is recommended by [11] to be used for calculations with strongly curved phase interfaces.

The PISO pressure-velocity coupling scheme, along with PRESTO! for pressure and bounded central differencing for density, momentum, and energy discretization, were used. Second-order implicit transient formulation is used along with the activation of recommended setting optimization for increased solution stability.

2.1 Geometry model

An effervescent atomizer with an outside-in air delivery was chosen for the study. The area of interest is mainly the mixing chamber, the air and water inlet channels, the outlet port, and its vicinity. The mixing chamber is cylindrical with 8 air inlet ports, an axial water inlet, and an axial discharge orifice. It is essential not to affect the region of interest by the presence of boundary conditions, so the air inlet channels have a length equal to 2 times the diameter, and the water inlet channel a length equal to 3 times the diameter. The ambient atmosphere is modeled as a cylinder with a radius of 5 mm and a length of 10 mm. This is to give the air enough time and space to expand to the ambient pressure. In order to maintain a realistic flow, the model does not use the symmetry assumption.

The geometry as shown in Figure 2, with the mixing chamber having a diameter of 10 mm and a length of 41 mm. The discharge orifice has a diameter of 2 mm and a length of 2 mm. The water inlet has a diameter of 6 mm. The air inlet ports have a diameter of 2 mm; the first is positioned 18 mm from the bottom, and they are spaced 6 mm apart.

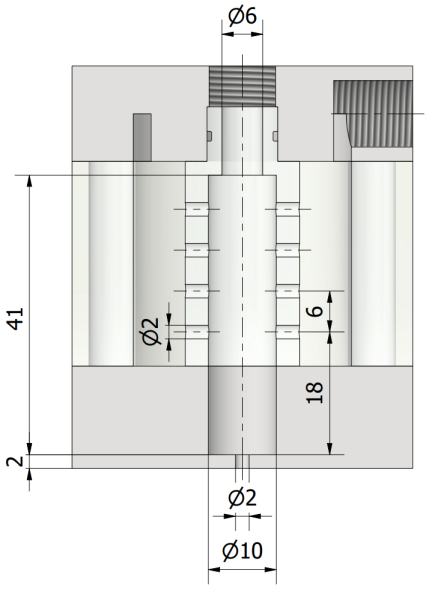

Figure 2: Simulated atomizer geometry (all dimension in millimeters)

2.2 Boundary conditions

Air and water are considered as an ideal gas and incompressible liquid with density linearly dependent on temperature. Their equations of state are 9 and 10, respectively,

$$\rho_g = \frac{pM_g}{R_m T} \tag{9}$$

$$\rho_l = \rho_{l0}[1 - \beta(T - T_0)] \tag{10}$$

where M_g is the molar mass of air, $R_m = 8.3143 \frac{J}{K \cdot mol}$ is the universal gas constant, $\beta = 2.1 \cdot 10^{-4} K^{-1}$ is the volume expansion coefficient, and $\rho_{l0} = 997 \frac{kg}{m^3}$ is the water density at temperature $T_0 = 20°C$.

In Figure 3 the geometric model of the domain is shown with the surfaces with specified boundary conditions being highlighted. The problem is defined using a mass flow inlet of water at 68.45 kg/h and a mass flow inlet of air at 0.64 kg/h. These boundary conditions allow a faster development of the velocity profile while allowing a non-uniform flow through each inlet depending on the back pressure at each position. Thus, the nozzle is operated at a gas to liquid ratio (GLR) of 0.93 percent. A static pressure condition allowing recirculation at 100 kPa is used for the ambient atmosphere definition. The simulation does not consider the influence of gravity.

2.3 Mesh

To ensure sufficient accuracy of the integration scheme capturing the interfacial interface, the calculation uses a tetra-hexcore mesh. This provides uniform hexahedral elements in volume. The transition of the hexahedral mesh to the wall is handled by the use of a transition layer of tetrahedral elements. The network does not include prismatic elements to describe the boundary layer flow, since the flow inside the mixing chamber does not appear to be susceptible to viscous forces introduced by friction against the wall, but is much more affected by viscous forces between the phases.

The element size is set based on a steady-state computation using a realizable k-ϵ turbulence model. The outcome of this computation is a distribution of variable k. Based on this variable, the size of the expected turbulent eddies is calculated. This calculation aims to simulate 80 percent of the turbulent eddies' energy. According to [10], to capture this amount of energy, it is recommended to use elements of one-fifth the size of the integral length scale from the equation 11.

$$L_t = \frac{k^{\frac{3}{2}}}{\epsilon} \tag{11}$$

The equation 11 is based on [9] and k represents the turbulent kinetic energy, and ϵ the rate of dissipation of turbulent kinetic energy.

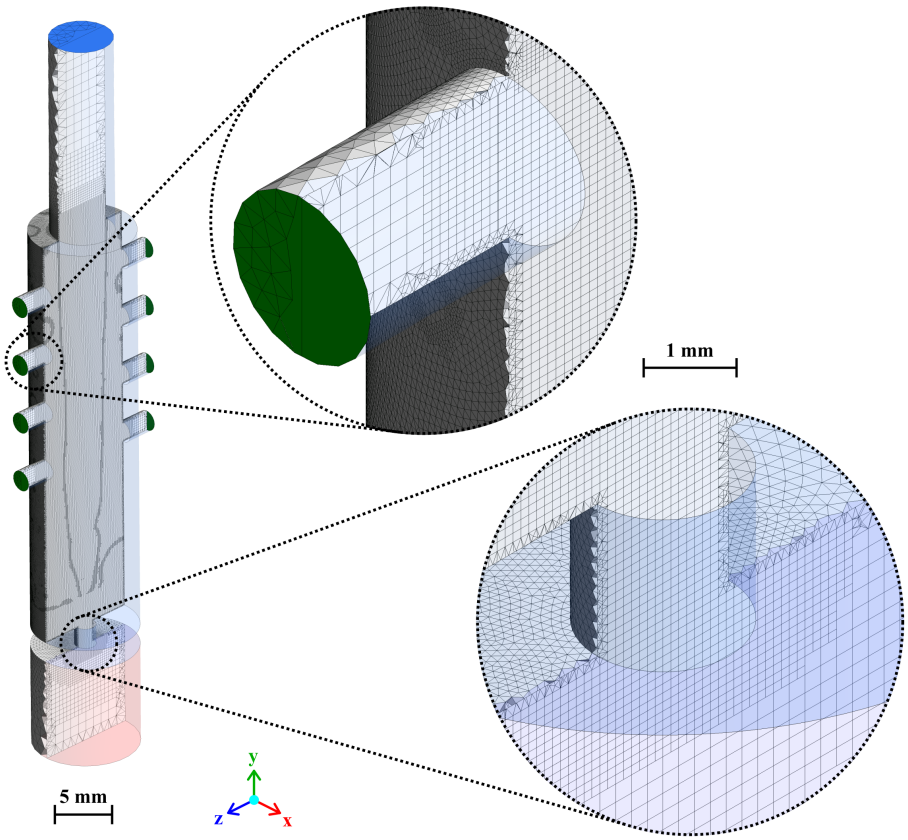

Figure 3: Computational domain with boundary conditions (blue - water inlet, green - air inlet, red - outlet) and mesh visualization.

The adaptive mesh refinement function is also used in the calculation, where the volume fraction gradient is considered an objective function. In case the value of this gradient function is too large within an element, the element is bisected. This study aims to capture droplets and bubbles of diameter larger than 0.2 mm. To achieve this, [6] recommends a resolution of 8 elements per feature thickness. This resolution is achieved by splitting initial elements once. In order to lower the Courant-Friedrichs-Lewy condition (CFL) in the discharge orifice and increase the solution stability, adaptive mesh refinement is not used near the discharge.

3 Results and discussion

First, a steady-state single-phase simulation was performed using only compressed air. This was then used as initial conditions for a transient two-phase simulation including water flowing through the central inlet. After the water column reached the bottom, a steep spike in internal pressure appeared. This created periodic pressure waves in the mixing chamber. The simulation was run until a point where the pressure waves stabilized, and 3 consecutive similar waves were tracked.

Because the main objective of this simulation was to prepare realistic parameters for the inlet boundary condition for the detailed discharge simulation, it was not necessary to describe the whole domain accurately, but mainly to capture the flow structures in the mixing chamber and its pressure. To maintain the accurate description of these structures, a maximum CFL value of 0.2 was considered in the mixing chamber, which corresponded to a time step of 7E-6 s due to the low velocities. At this time step, however, the CFL in the outlet reached 20 and it was not possible to precisely define the interface there, which can be seen in detail in Figure 6. But in this case, the only property of the outlet that needs to be described precisely is the pressure drop.

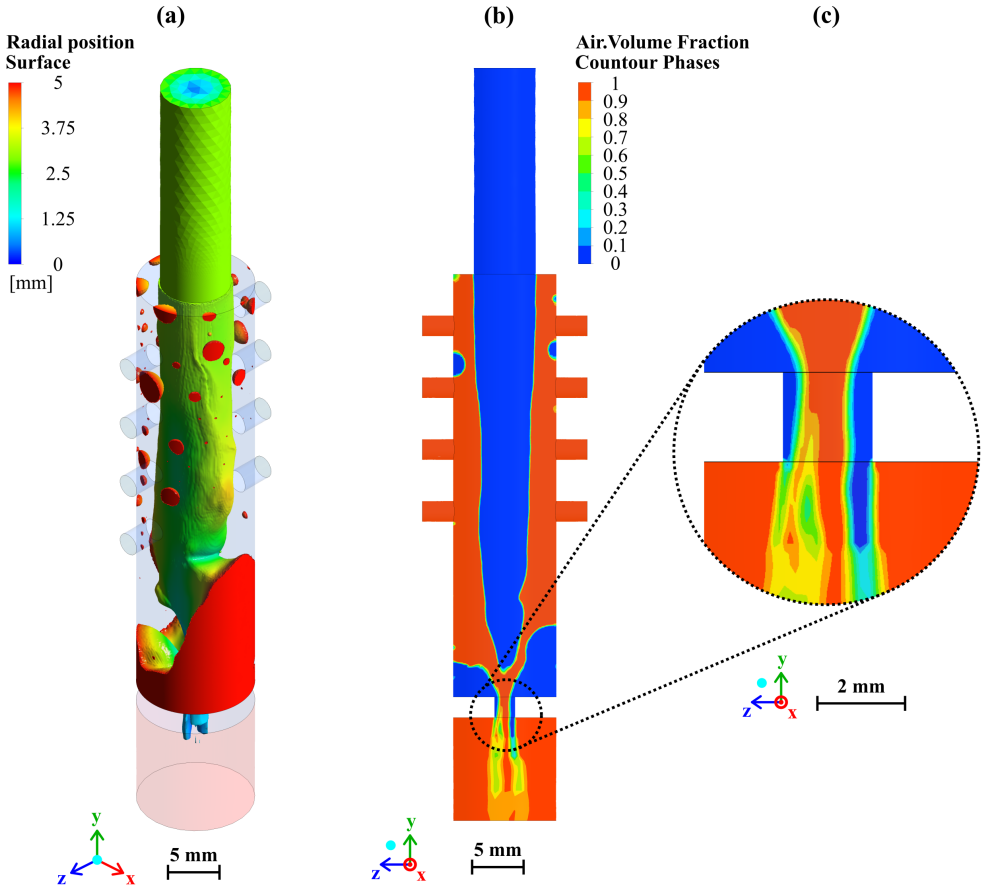

Figure 4: Flow structures inside the atomizer in 3D with radial position as contour variable (a) and cross-section with air volume fraction as contour variable (b), with detail of the discharge orifice (c).

As can be seen in Figure 6, the flow inside the mixing chamber had the character of an axial jet of liquid, which was not broken by air jets. This flow was only broken at the bottom of the chamber, where it formed a sloshing region of liquid at the corners around the perimeter. From this, water was then drawn together with air into the discharge orifice. At the same time, water droplets were retained on the cylinder liner. Because of a coarse mesh near the walls, the simulation did not capture the thin film wetting the cylinder walls.

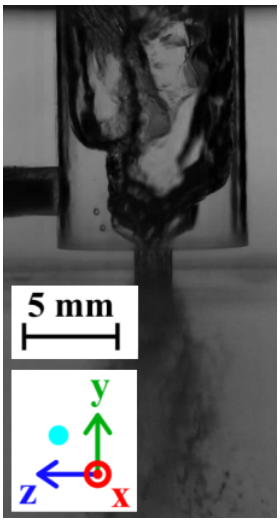

Figure 5: Experimental measurement of the same atomizer during the same conditions

In the experimental measurements shown in Figure 5, similar flow structures were qualitatively comparable, and the measured relative pressure in the atomizer was 102.3 $\pm$ 2 kPa . The static relative pressure in the mixing chamber according to the simulations was 80.3 kPa, as can be seen in Figure 6. Thus, a deviation of 21.5 percent is observed. In both cases, the pressure value showed a fluctuation with an amplitude of 10 kPa. These were most probably caused by the sloshing of the flow structures. The pressure deviation was probably due to insufficient resolution of the boundary layer modeling and the outlet opening having too large a throughput.

Figure 6 (a) also displays a match between simulated and expected pressure difference inside liquid structures caused by the surface tension based on 12,

$$\Delta p_{cyl} = \frac{2\sigma}{D_{cyl}} \tag{12}$$

where p_{cyl} is the increase in pressure inside the liquid jet and the D_{cyl} is the jet diameter. Analytical formula without considering change in momentum gives $\Delta p = 24$ Pa at the water inlet, whereas simulation gave $\Delta p = 22$ Pa.

Figure 6 (b) shows that in this regime, the gas flow field was relatively streamlined, as the strong vorticity seemed to be mainly around the first pair of air inlet channels, where the streamlines formed a helix. After that, gas mostly steadily flowed into the discharge. Figure 6 (c) shows that the majority of the water introduced into the atomizer flowed directly into the discharge and did not replace the water contained in the corner at the bottom of the mixing chamber. Over 90 percent of the liquid introduced into the domain leaves it in under 100 ms.

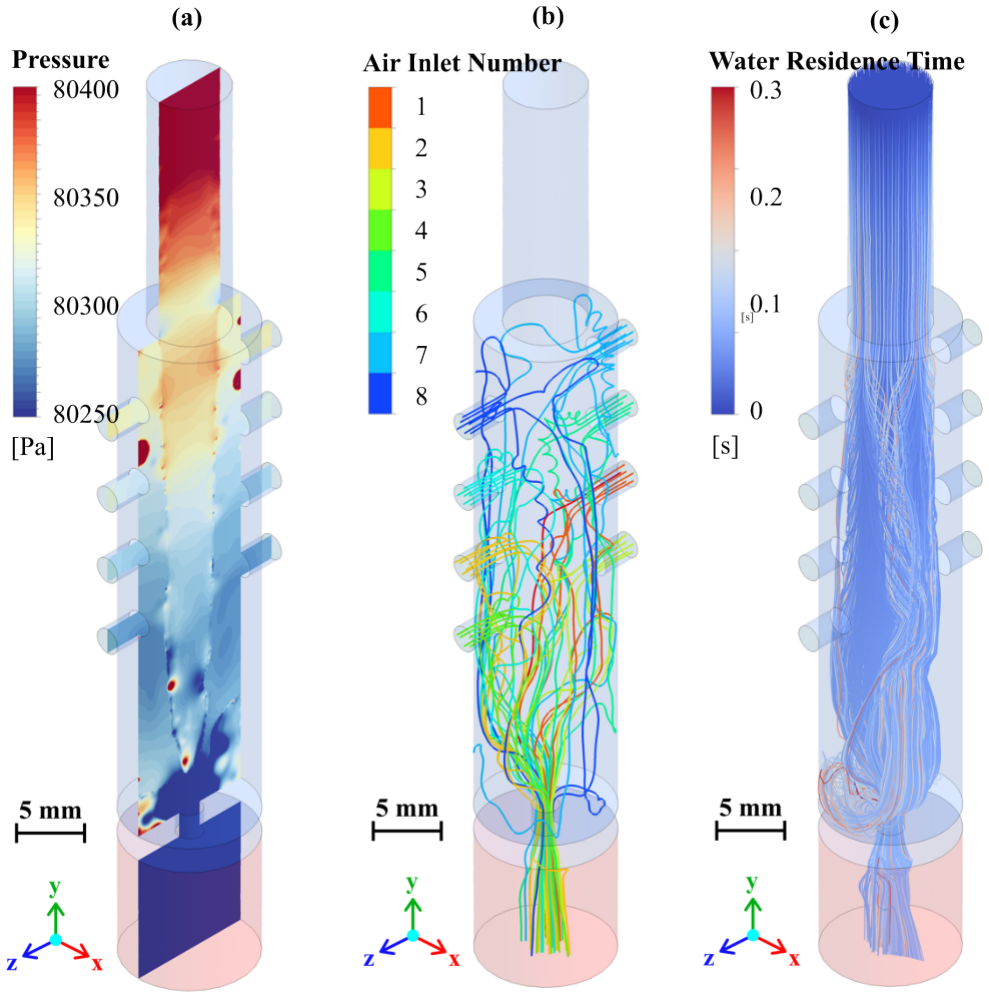

Figure 6: Pressure field inside the atomizer (a), streamlines originating in air inlet boundary condition (b), streamlines originating in water inlet boundary condition (c)

4 Conclusion

Studying the behavior of internal mixing atomizers using experimental measurements is often limited by the achievable detail. It is therefore an option to investigate these phenomena through computational flow simulations. This study utilizes the finite volume method in conjunction with the Volume of Fluid model and Large Eddy Simulation. Through simplified calculations, it selects an optimized computational mesh, which is further modified by Automatic Mesh Refinement at the interface. The mass flow rates of the different fluids are considered as inlet parameters.

The area of interest is mainly the atomizer discharge orifice. However, due to the computational complexity of simulating the whole atomizer with precise flow behavior in the discharge orifice, the problem is divided into two parts. The simulation results contained in this paper will be used as an inlet boundary condition for a detailed model of the atomizer discharge orifice.

For the same atomizer geometry, the internal flow structures were investigated experimentally using a high-speed camera along with the pressure measurement. The simulation results were qualitatively comparable with the high-speed recordings. The pressure inside the atomizer was 21 percent lower in the simulation than in the experimental measurements while displaying similar fluctuations.

It can be concluded that the simulation shows correct trends and behaves similarly to an experimental atomizer. An area for improvement seems to be the boundary layer modeling at the discharge orifice, which has an inadequate pressure ratio at specified mass flow rates.

Acknowledgment

The authors acknowledge the financial support from the project no 23-07722S funded by the Czech Science Foundation and by the project FSI-S-23-8192 funded by the Brno University of Technology.

References

[1] Sun, C., Ning, Z., Qiao, X., Lv, M., Li, Y., Zhao, J. & Wang, X.: Measurements of internal flow regime and bubble size in effervescent atomizer. *Experimental Thermal and Fluid Science*, (2018), https://doi.org/10.1016/J.EXPTHERMFLUSCI.2018.07.002.

[2] Hammad, F., Sun, K., Che, Z., Jedelský, J. & Wang, T.: Internal two-phase flow and spray characteristics of outside-in-liquid twin-fluid atomizers. *Applied Thermal Engineering*, vol. 187, 116555, (2021) https://doi.org/10.1016/J.APPLTHERMALENG.2021.116555.

[3] Law, D., Shepard, T. & Wardi, I.: A Combined Numerical and Experimental Study of Air Bubble Dynamics in Converging Section of Effervescent Atomizer. *ASME-JSME-KSME Joint Fluids Engineering Conference* (2015) https://doi.org/10.1115/AJKFLUIDS2015-21100.

[4] Sun C., Ning Z., Qiao X., Lv M., Fu J., Zhao J. & Wang X.: Numerical simulation of gas–liquid flow behavior in the nozzle exit region of an effervescent atomizer. *International Journal of Spray and Combustion Dynamics*, vol. 11, (2019), DOI:10.1177/1756827718821592

[5] Esfarjani, S. & Dolatabadi, A.: A 3D simulation of two-phase flow in an effervescent atomizer for suspension plasma spray. *Surface Coatings Technology*, vol. 203, pp. 2074-2080, (2009), https://doi.org/10.1016/J.SURFCOAT.2008.10.024.

[6] Kant, P., Pairetti, C., Saade, Y., Popinet, S., Zaleski, S. & Lohse, D.: Bag-mediated film atomization in a cough machine. *Physical Review Fluids*, vol. 8, (2023), https://doi.org/10.1103/physrevfluids.8.074802.

[7] Salvador, F., Romero, J., Roselló, M. & Jaramillo, D.: Numerical simulation of primary atomization in diesel spray at low injection pressure. *Journal of Computational and Applied Mathematics*, vol. 291, pp. 94-102, (2016), https://doi.org/10.1016/j.cam.2015.03.044.

[8] Spalart P. R.: Young-Person's Guide to Deteched-Eddy Simulation Grids. NASA/CR-2001-211032. (2001)

[9] Menter F. R.: Best Practice: Scale-Resolving Simulations in ANSYS CFD, version 2.00. Available from ANSYS Customer Portal. (2015)

[10] Gerasimov A.: Quick Guide to Setting Up LES-type simulations, version 1.4. Available from ANSYS Customer Portal. (2016)

[11] ANSYS, Inc. ANSYS Fluent Theory Guide. ANSYS Inc., Canonsburg. (2020)